Small-angle X-ray scattering shape metrology for 3D semiconductor devices

Takumi Goto*

Abstract

The etching technique for high-aspect-ratio hole structures is one of the key technologies in modern semiconductor device manufacturing. Accurately evaluating hole shapes is crucial for developing and controlling the etching process. In order to create a precise evaluation system for deep hole shapes, Rigaku has developed a transmission small-angle X-ray scattering (T-SAXS) instrument. In this technical note, we describe the principles of a small-angle X-ray scattering (SAXS) technique for the determination of three-dimensional semiconductor device structures and its measurement sensitivity based on simulation results. We also demonstrate its performance for SAXS metrology by the measurement of deep holes on a 300 mm wafer. As a result of these measurements we were able to obtain the distribution of deep hole sizes and their tilt across the entire wafer.

1. Introduction

The evolution of digital technology has been remarkable over the past few years. Artificial intelligence, driverless cars, metaverse, and other new digital technologies that once existed only in the world of science fiction are now being realized in the real world and are bound to enrich our social lives. In order to realize such digital technologies, high-performance semiconductor devices are indispensable.

The performance improvement of semiconductor devices has been achieved by miniaturizing device scale and increasing their integration rate. However, the limits of physical miniaturization were being reached. Therefore, three-dimensional stacked device structures have become the mainstream in current semiconductor development and manufacturing. For instance, in the case of NAND flash memory, a structure with approximately 200 layers of memory cells has been developed and is already available on the market.

One of the manufacturing processes for these devices involves the fabrication of high-aspect deep holes that reach several micrometers in depth with a diameter of approximately one hundred nanometers. The deep hole shape is directly related to the quality of the device. If the deep holes are not fabricated as designed, or if there are large variations in shape, the maximum performance of the device will not be achieved. Therefore, the deep hole etching process is positioned as one of the important technologies in modern semiconductor manufacturing. Shape parameters that characterize the deep hole structures include the diameter (critical dimension: CD), tilt, and depth of deep holes. It is very important for modern etching process to control these parameters across an entire wafer. The etching process is optimized based on the measurement results of the hole shape. Therefore, highly accurate shape measurement technology is essential for process control. Optical critical dimension spectroscopy (OCD), scanning electron microscopy (SEM), and transmission electron microscopy (TEM) are generally used to measure the deep hole shapes. OCD has advantages in terms of measurement throughput. However, due to the characteristics of the probe wavelength, measuring hole shapes that are several microns deep with high resolution is challenging. SEM and TEM can obtain actual images with high resolution, but they require destruction of the sample. Furthermore, their field of view is too small to be suitable for measuring the whole wafer.

SAXS is well-known as a nondestructive shape measurement method. Around the year 2000, research into the shape measurement of semiconductor devices using SAXS commenced[(1)]. Rigaku launched XTRAIA CD-3000G, a grazing incidence small-angle X-ray scattering (GI-SAXS) system, for semiconductor manufacturing facilities. GI-SAXS has been utilized to measure the shapes of planar memory devices, photoresist patterns, and nanoimprint patterns with depths of approximately one hundred nanometers[(2)–(4)]. However, in the grazing incidence geometry, it is impossible for X-rays to penetrate to the bottom of a deep hole several micrometers in depth due to X-ray absorption. On the other hand, by employing the transmission geometry with short wavelength X-rays, the substrate can be effectively penetrated by X-rays, which enables us to measure deep hole shapes. Therefore, Rigaku have developed a new instrument featuring a transmission-type small-angle scattering (T-SAXS) geometry and launched it in 2020.

In this technical note, we introduce the fundamental measurement principles of small-angle X-ray scattering. Additionally, we present the results of shape measurements of a 1 μm deep hole structure pattern formed on the surface of a 300 mm silicon wafer, along

* X-ray research laboratory, Rigaku Corporation.

with an evaluation of the etching properties across the entire wafer.

2. Principle of Transmission-type Small-angle X-ray Scattering

The use of SAXS in transmission geometry enables the measurement of deep holes with depths of several micrometers. Figure 1 shows the measurement geometry for T-SAXS. When X-rays are irradiated onto an object with an electron number density distribution $\rho(\boldsymbol{r})$, incident X-rays are scattered. The scattering intensity $I(\boldsymbol{Q})$ is given by the square of the absolute value of the Fourier transform of $\rho(\boldsymbol{r})$, as shown in Eq. (1), where $\boldsymbol{Q}$ is the scattering vector in reciprocal space. In particular, X-ray diffraction spots are observed when the object has a periodic structure. As shown in Fig. 1, when the unit cell of the periodic structure has lattice constants of a and b, and a lattice angles of θ, the diffraction condition can be expressed by Eq. (2). Each diffraction spot is identified by a set of the diffraction indices h and k. Q_X, Q_Y, and Q_Z are defined as scattering vector components horizontal to the a-axis, perpendicular to the a-axis, and normal to the wafer surface, respectively.

By using a two-dimensional detector, the X-ray intensities of multiple diffraction points that satisfy the diffraction conditions can be collected simultaneously. The scattering vector Q_R is defined as $Q_R=\sqrt{Q_X^2+Q_Y^2}$. The scattering intensity data as a function of Q_R shown in the top left of Fig. 1 is the integrated intensity of each diffraction spot at the vertical incidence condition. A periodic intensity profile is observed when the intensity of each diffraction point is plotted against the scattering vector Q_R on the horizontal axis. From this profile, information regarding the average CD of the X-ray irradiated area can be obtained. Details are described in Section 3.1. Next, to determine the three-dimensional structure, it is necessary to obtain information on the scattering vector Q_Z, which corresponds to the depth direction. When the sample is rotated by an angle ω, the scattering vector Q_Z changes as $Q_Z \approx -Q_X \tan\omega$. Multiple images are collected according to the rotation angle of the sample. By analyzing the dependence of the X-ray intensity at each diffraction point in the Q_Z direction, it is possible to determine the depth, shape, and tilt. The scattering intensity is calculated using a scatterer model with the shape parameters shown in Fig. 2. The calculated model is represented by dividing the scatterer into $N+1$ layers along the depth direction. Each layer has six parameters, which are the CD in the XY direction (Lx, Ly), the center positions of the cross-sectional shape in the XY direction (Dx, Dy), the layer thickness (t), and the electron number density of the side walls (ρ). These shape parameters are optimized using the least-squares method until the difference between the experimental and calculated scattering intensities is minimized.

$$I(\mathbf{Q}) = \left| \int_V \rho(\boldsymbol{r}) e^{-i\mathbf{Q}\cdot\boldsymbol{r}} d\boldsymbol{r} \right|^2 \tag{1}$$

$$Q_X = 2\pi\frac{h}{a},\ Q_Y = 2\pi\left(-\frac{h}{a\tan\theta}+\frac{k}{b\sin\theta}\right) \quad (h,k\text{: integer}) \tag{2}$$

3. Evaluation of Measurement Sensitivity Using SAXS Intensity Simulation

In this section, we discuss the effect on the scattering intensities when the shape of the scatterer is changed based on simulation results. The scatterers are a square lattice of deep holes with a pitch of 120 nm. The scattering intensity data is simulated in the rotation angle range of −18° to 18° at intervals of 0.06°. The

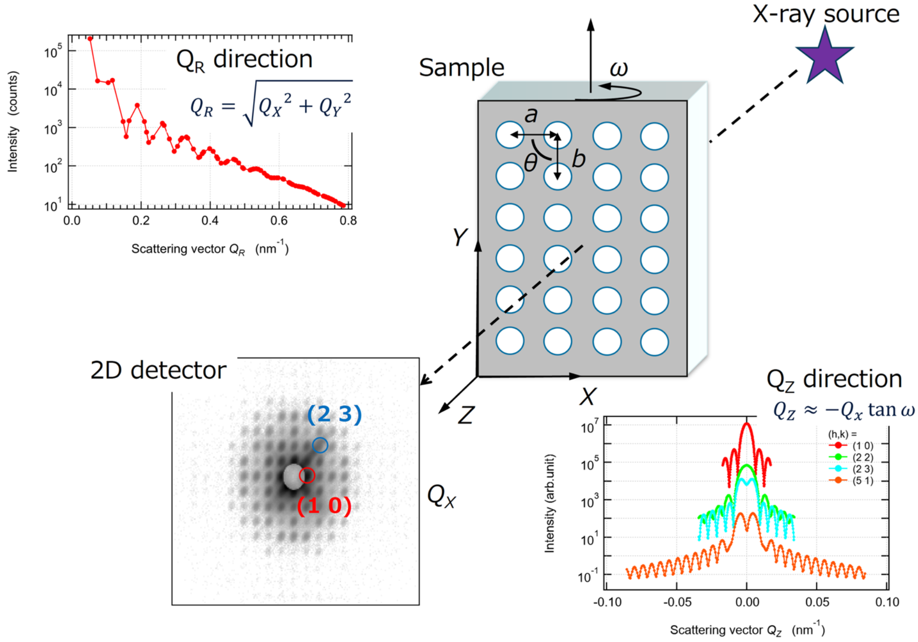

Fig. 1. Measurement geometry for transmission small-angle X-ray scattering.

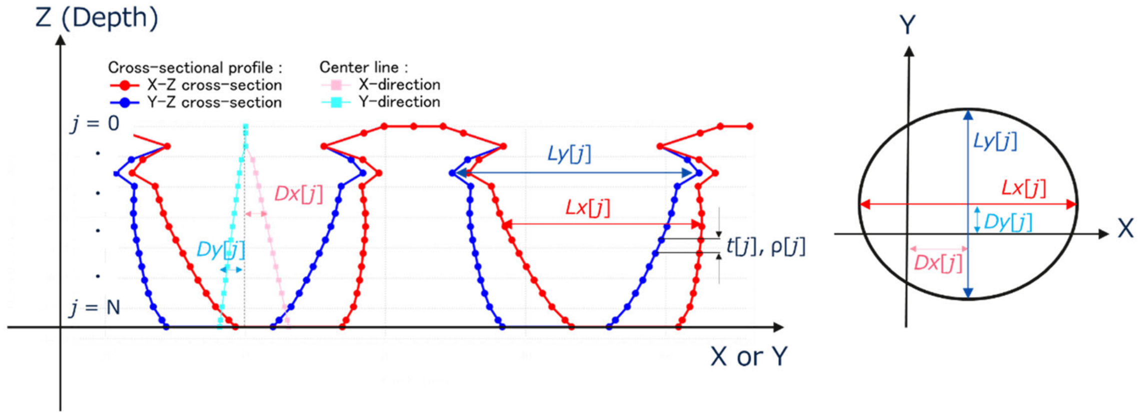

Fig. 2. Schematics of the analysis model.

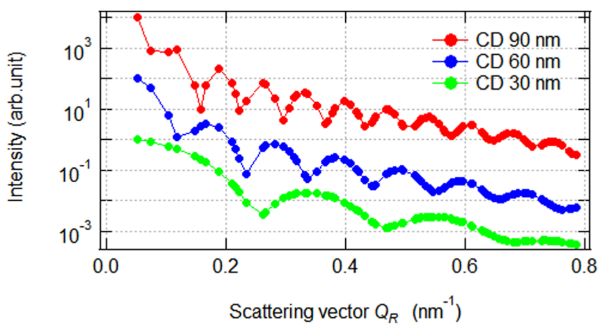

Fig. 3. Calculated intensities in the Q_R direction of a cylindrical hole with different CDs.

number of layers in the scattering model is set to 40 for all simulations. First, we focus on the sensitivity of the scattering intensity in the Q_R direction.

3.1 Simulation of SAXS intensity in the Q_R direction

First, we will explain the sensitivity of scattering intensity data in the Q_R direction to CD changes. Figure 3 shows the calculated intensities for CD of 30 nm, 60 nm, and 90 nm. The deep hole has a cylindrical shape and its depth is 1000 nm. The simulation data indicate that the fringe period decreases as the CD increases. There is a relationship between the fringe period (ΔQ_R) and the average CD ($CD_{Ave.}$): $CD_{Ave.} \approx 2\pi/\Delta Q_R$. Therefore, the scattering intensity in the Q_R direction is highly sensitive to the average CD.

3.2 Simulation of SAXS intensity in the Q_Z direction

3.2.1 Hole depth

Next, we will focus on the sensitivity of the scattering intensity data in the Q_Z direction. We will explain the sensitivity of scattering intensity data in the Q_Z direction to changes in the hole depth. Figure 4 shows the simulation data at the diffraction indices (1 0) and (2 3). Scattering intensities are calculated for hole depths of 500 nm, 1000 nm, and 2000 nm, respectively. The simulation data indicates that the fringe period of the scattering intensity at each diffraction point decreases as the hole depth increases. A relationship exists between the period of the scattering fringes in the Q_Z direction (ΔQ_Z) and the depth of the hole (*Depth*): $Depth \approx 2\pi/\Delta Q_Z$. Therefore, the period of the scattering fringes in the Q_Z direction is highly sensitive to the depth of hole.

3.2.2 Side wall angle

Next, we will explain the sensitivity of scattering intensity data in the Q_Z direction to changes in the sidewall angle. Figure 5 a) shows the simulation models. The first model is cylindrical with a side wall angle of 90°. The second model has a tapered shape with a side wall angle of 88°. Both models have a depth of 1000 nm and the average CD is 90 nm. Figures 5 (b) and (c) show simulation data for the cylindrical and the tapered shape, respectively. The scattering intensities obtained by the cylindrical hole show a maximum intensity at $Q_Z = 0\,\text{nm}^{-1}$ for all diffraction indices. Also, the period and phase of the fringes never change for all diffraction indices. On the other hand, the maximum scattering intensity obtained using the tapered model is not necessarily at $Q_Z = 0\,\text{nm}^{-1}$. A deviation of the sidewall angle from 90° has the effect of changing the phase of the scattered intensity data in the Q_Z direction. The higher the diffraction index, the larger the phase change. These simulation results indicate that the sidewall angle can be easily analyzed from the phase change and that the scattering intensity data has high sensitivity to sidewall angle changes.

3.2.3 Tilt angle

Finally, we will explain the sensitivity of scattering intensity data in the Q_Z direction to changes in the tilt angles. Figure 6 a) shows the simulation models. The tilt angles in the X direction are −0.5°, 0°, and 0.5°, respectively. For all three models, the depth is 1000 nm and the average CD is 90 nm. The simulation data obtained from each model are overlaid in Figure 6 (b). When the tilt angle is 0°, the simulation data is symmetrical about $Q_Z = 0\,\text{nm}^{-1}$. On the other hand, if the tilt angle is not 0°, the center of symmetry shifts from $Q_Z = 0\,\text{nm}^{-1}$. This behavior differs from the phase changes that occur depending on the sidewall angle,

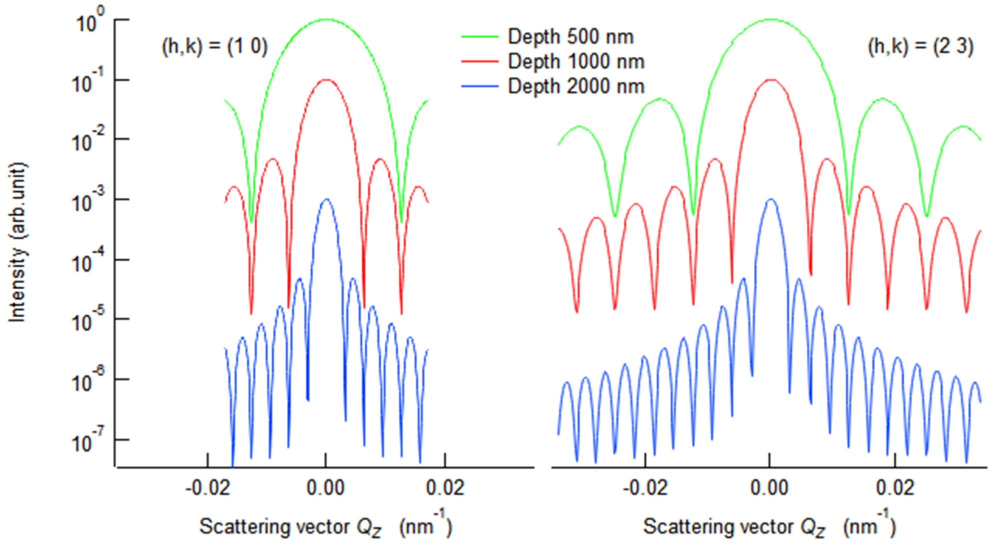

Fig. 4. Calculated intensities in the Q_Z direction of a cylindrical hole with different depths.

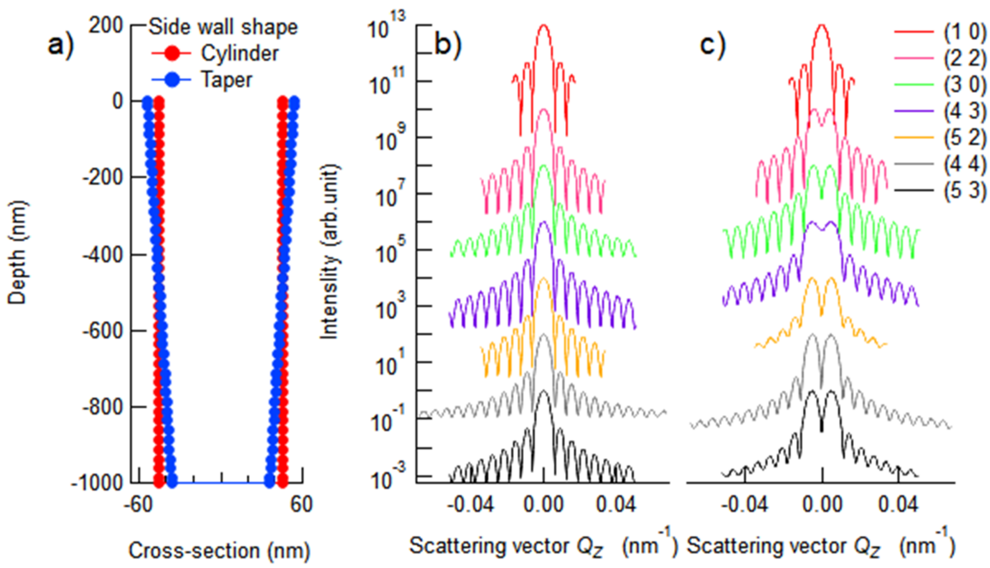

Fig. 5. Calculated intensities in the Q_Z direction of a cylindrical hole with different side wall angles.
a) Simulation model, b) and c) represent the calculated scattering intensities of the cylindrical and tapered holes, respectively.

as described in Section 3.2.2. There is a relationship between the shift of the center of symmetry ($Q_{Z\ shift}$) and the tilt angles (θ_X, θ_Y) in the X and Y directions: $Q_{Zshift}=-Q_X \tan\theta_X - Q_Y \tan\theta_Y$. The tilt angles can be determined from the magnitude of the shift of the center of symmetry in the Q_Z direction.

Summarizing the results of the previous simulations, it can be concluded that T-SAXS is highly sensitive to variations in CD, depth, sidewall angle, and tilt angle. The T-SAXS measurement technique can accurately determine the shape parameters essential for characterizing high-aspect deep holes.

4. Measurement of Deep Hole Patterns Formed on 300 mm Wafers

4.1 Equipment

In this section, we report the measurement results for 1 μm deep holes formed on a 300 mm wafer. Figure 7 shows the XTRAIA CD-3000T instrument employing T-SAXS developed by Rigaku. Because the X-rays need to penetrate a silicon wafer approximately 800 μm thick, a rotating molybdenum target (X-ray wavelength: 0.071 nm) is selected as the X-ray source. An X-ray mirror is used to monochromatize and focus the X-rays. X-rays are irradiated from the back of the wafer and pass through the apparatus from the lower side to the upper side. The intensities of the scattered X-rays are collected using a large-area hybrid two-dimensional

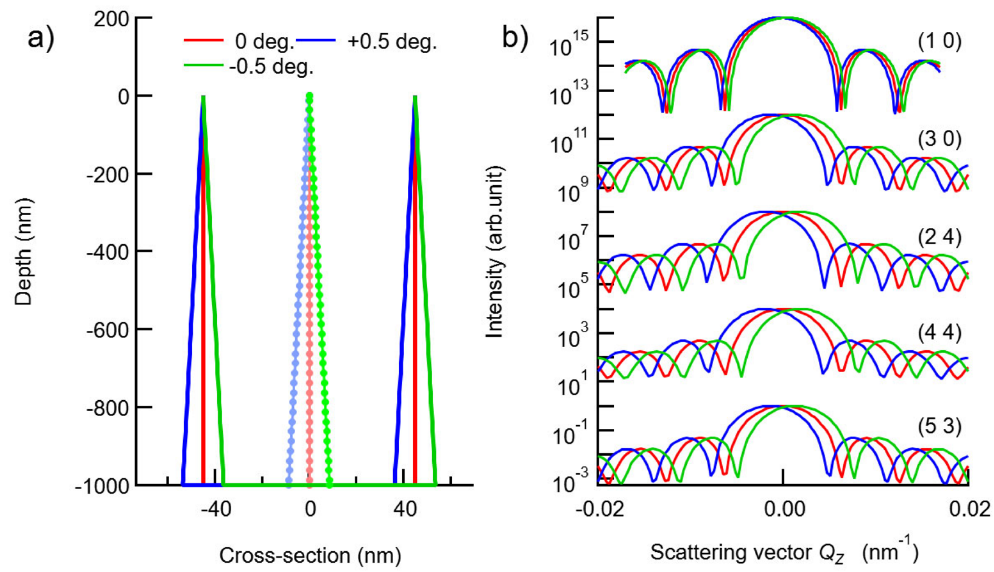

Fig. 6. Calculated intensities in the Q_Z direction of a cylindrical hole with different hole tilts.
a) Simulation model, b) simulation results of scattering intensity in the Q_Z direction. The red, blue, and green lines show simulation results for tilt angles of 0°, +0.5°and −0.5°, respectively.

Fig. 7. Rigaku XTRAIA CD-3000T inline T-SAXS metrology tool.

detector (HyPix6000 HE) mounted on the top of the instrument. A visible light tilt sensor is utilized to measure the warpage of a wafer surface and to calibrate the angle of incidence of the X-rays to the wafer.

4.2 Deep hole pattern measurement and 3D shape analysis

A sample with a deep hole pattern etched on the surface of a 300 mm wafer was prepared. The deep holes are a periodic square lattice pattern with a pitch of 120 nm, and 64 chips are fabricated on the 300 mm wafer. The wafer was rotated from −18° to 18°, and X-ray scattering intensity images were acquired at 0.06° intervals. The X-ray irradiation time per measurement point is 10 minutes.

Figure 8 a) and b) show the observed and calculated intensities at the chip located in the center of the wafer. In this analysis, the deep hole was divided into 40 layers along the depth direction, and the shape parameters of each layer were optimized using the least squares method. Figure 8 c)–e) show the results of the analysis of the deep hole shape. The depth of the deep hole was 1017 nm and the average CD was 80.9 nm. The CD tends to decrease toward the bottom of the hole, and the sidewall angle is calculated as 87.9° from the CD profile. Additionally, the CD profile has a bowing shape at a depth of approximately 200 nm from the surface. The center line is nearly at 0 nm, indicating that there is no tilt in the deep hole formed at the center of the wafer.

Figure 9 shows the observed and calculated intensities at the chip located on the left edge of the wafer, along with the corresponding analysis results. The CD profile of the left-edge chip is similar to that of the center chip. However, the average CD is 87.7 nm, which is 6.8 nm larger than that of the center chip. Figure 9 a) shows a significant change in the phase of the scattered intensity. The analysis results show that the holes are etched with a tilt of 0.52° in the X-direction of the wafer.

4.3 Evaluation of etching properties across the entire wafer.

Figure 10 shows the distribution of the average CD obtained from measurements of all 64 chips on the wafer. It is clear that the average CD of deep holes increases from the right side to the left side of the wafer. Finally, we show the trend of hole tilt angles across the entire wafer. Figure 11 a) is a vector map of the observed hole tilt. The measurement results indicate that nearly every hole has an outward tilt. Figure 11 b) shows the results of plotting the tilt angle, which has been converted into the radial and tangential components of the wafer. The horizontal axis is the radius of wafer. The tilt angle is oriented in the radial direction, and increases

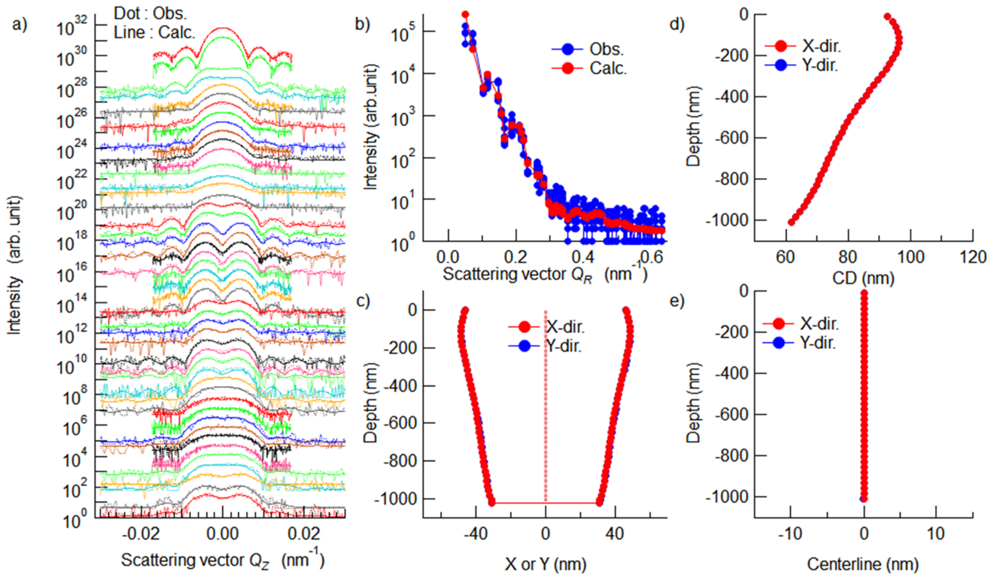

Fig. 8. Measurement and analysis results of deep hole patterns formed on the center of the wafer. a) and b) are observed and calculated intensity in Q_Z and Q_R direction, respectively. Analysis results of c) cross section profile, d) CD profile and e) centerline profile.

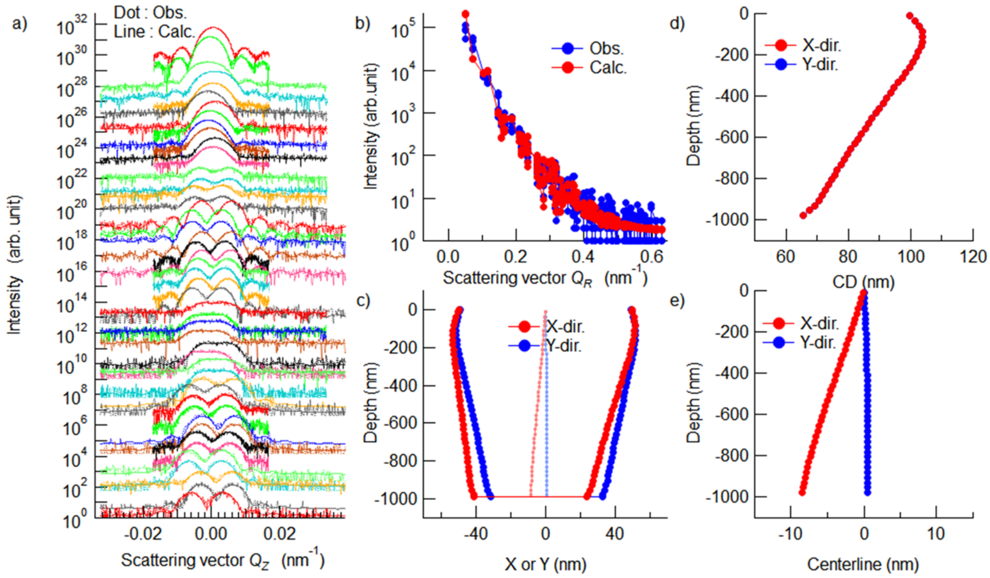

Fig. 9. Measurement and analysis results of deep hole patterns formed on the left edge of the wafer. a) and b) are observed and calculated intensity in Q_Z and Q_R direction, respectively. Analysis results of c) cross section profile, d) CD profile and e) centerline profile.

toward the edge of wafer.

These results demonstrate that T-SAXS has enough performance to characterize the CD, depth, and tilt angle of deep holes. Furthermore, because T-SAXS is a nondestructive measurement technique, it enables the evaluation of the distribution of shape parameters across the entire wafer. It is expected that shape measurement by T-SAXS will contribute to the optimization of etching equipment.

5. Conclusion

We introduced small-angle X-ray scattering shape metrology for 3D semiconductor device structures. Simulation-based discussions indicate that this metrology has sufficient sensitivity to determine shape parameters, which are essential for characterizing high-aspect semiconductor structures. We also measured the deep hole patterns on a 300 mm wafer. As a results of these measurement, the detailed 3D shape of the deep holes could be accurately determined. Additionally, the characteristic changes in average CD and hole inclination across the entire wafer were obtained. SAXS measurements are highly effective for evaluating shape parameters that are important for controlling the etching process of deep hole structures. This measurement method is capable of analyzing complex 3D shapes,

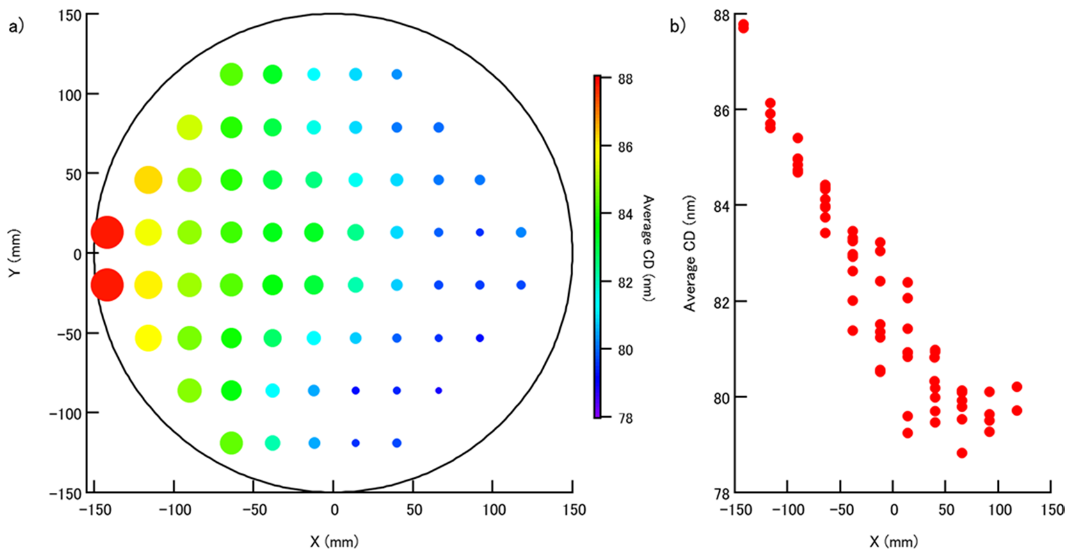

Fig. 10. a) Color scale map of average CD. b) The graph of average CD across the entire wafer with the wafer X position plotted on the horizontal axis.

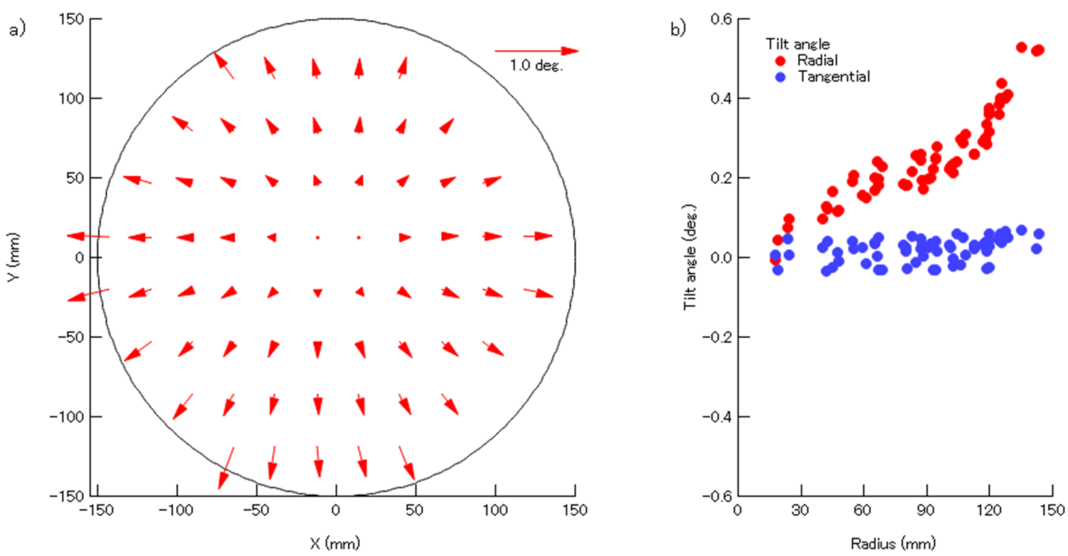

Fig. 11. a) Vector map showing the hole tilt magnitude and direction across the entire wafer. The arrow tip indicates the bottom direction of deep holes. b) The graph shows hole tilt angle distribution across the entire wafer. Red and blue dot represent radial and tangential tilt angles, respectively.

such as pillars, slits, liner film profiles[6], and X-Y cross-sectional shapes[7]. Semiconductor devices featuring high-aspect structures include channel holes and slits in 3D NAND, capacitor holes in DRAM, and trench structures in CMOS imaging sensors. The SAXS method, which can nondestructively measure these structures with high accuracy, is anticipated to be a highly valuable technique for evaluating semiconductor devices with 3D structure. As semiconductor device structures evolve into three-dimensional structures, we expect that X-ray measurement technology will be employed across various fields, including device development and quality control.

Reference

(1) W. Wu, R. J. Kline, R. L. Jones, H. J. Lee, E. K. Lin, D. F. Sunday, C. Wang, T. Hu and C. L. Soles, *J. Micro/Nanopattern. Mater. Metrol.*, **22(3)** (2023), 031206, 1–15.

(2) K. Omote, Y. Ito and Y. Okazaki, *Proc. SPIE* **7638** (2010), 763811, 1–8.

(3) Y. Ito, A. Higuchi and K. Omote, *Proc. SPIE* **9778** (2016), 97780L, 1–8.

(4) E. Yamanaka, R. Taniguchi, M. Itoh, K. Omote, Y. Ito, K. Ogata and N. Hayashi, *Proc. SPIE* **9984** (2016), 99840V, 1–8.

(5) Y. Ito, T. Goto, R. Suenaga and K. Omote, *Jpn. J. Appl. Phys.* **62**(2023), 046501, 1–6.

(6) R. Suenaga, Y. Ito, T. Goto and K. Omote, *Proc. SPIE* **12496**(2023), 12496A, 1–7.

(7) R. Suenaga, Y. Ito, T. Goto and K. Omote, *Jpn. J. Appl. Phys.* **62**(2023), 096502, 1–8.